ADVANCED PHYSICS RESEARCH Open Access
www.advphysicsres.com

InAs–InP Superlattice Nanowires with Tunable Phonon Frequencies

V. Zannier, J. Trautvetter, A. K. Sivan, F. Rossi, D. de Matteis, B. Abad, R. Rurali, L. Sorba, and I. Zardo**

The control of heat conduction through the manipulation of phonons in solids is of fundamental interest and can be exploited in applications for thermoelectric conversion. In this context, the advent of novel semiconductor nanomaterials with high surface-to-volume ratio, e.g. nanowires, offer exciting perspectives, leading to significant leaps forwarding the efficiency of solid-state thermoelectric converters after decades of stagnation. Beyond the high aspect ratio, the nanowire geometry offers unprecedented possibilities of materials combination and crystal phase engineering not achievable with 2D counterparts. In this work, the growth of long (up to 100 repetitions) wurtzite InAs/InP superlattice nanowires with homogeneous segment thicknesses is reported, with control down to the single digit of nanometer. By means of Raman scattering experiments, clear modifications of the phonon dispersion in superlattice nanowires are found, where both InAs-like and InP-like modes are present. The experimentally measured modes are well reproduced by density functional perturbation theory calculations. Remarkably, it is found that the phonon frequencies can be tuned by the superlattice periodicity, opening exciting perspectives for phonon engineering and thermoelectric applications.

1. Introduction

Semiconductor nanowires (NWs) offer many possibilities to engineer systems at the nanoscale by controlling the size, the crystal structure, the chemical composition, and by combining different materials or crystal phases in heterostructures that cannot be realized in conventional geometries.[1,2] Remarkably, the growth of dislocation-free heterostructures of highly mismatched materials can be obtained in free-standing NWs, thanks to the strain relaxation on the sidewalls, along the growth axis.[3] This is particularly interesting for the realization of quantum dots (QDs) and superlattices (SLs), providing a great opportunity to explore new optical, electrical, and vibrational properties.

Superstructures consisting of a periodic arrangement of two materials, i.e., SLs, can successfully exploit wave interference phenomena, such as the formation of forbidden electronic and phonon bandgaps and the modification of the density of electronic states and group velocities of phonons, representing a promising platform to control and tune the thermal properties of materials.[4–7] However, the lattice mismatch has strongly limited their development in 2D growth. In fact, bulk SLs have been realized by combining lattice-matched materials like GaAs/AlAs,[4] GaAsSb/InGaAs[8] or InP/InGaAs[9] and nearly-lattice-matched systems like InAs/GaSb,[10] and InAs/InAsSb.[11] Nevertheless, very few reports can be found on InAs/InP SLs,[12,13] due to the lattice mismatch between InAs and InP (3.2%). On the other hand, InAs/InP SLs are very attractive both for fundamental studies and for applications in long-wavelength (1–2 μm) optoelectronic devices.[14,15]

V. Zannier, L. Sorba
NEST
Istituto Nanoscienze-CNR and Scuola Normale Superiore
Piazza San Silvestro 12, Pisa I-56127, Italy
E-mail: valentina.zannier@nano.cnr.it

The ORCID identification number(s) for the author(s) of this article can be found under https://doi.org/10.1002/apxr.202300157

© 2024 The Authors. Advanced Physics Research published by Wiley-VCH GmbH. This is an open access article under the terms of the Creative Commons Attribution License, which permits use, distribution and reproduction in any medium, provided the original work is properly cited.

DOI: 10.1002/apxr.202300157

J. Trautvetter, A. K. Sivan, D. de Matteis, B. Abad, I. Zardo
Physics Department
University of Basel
Klingelbergstrasse 82, Basel CH-4056, Switzerland
E-mail: ilaria.zardo@unibas.ch

F. Rossi
IMEM-CNR
Parco Area delle Scienze 37/A, Parma I-43124, Italy

R. Rurali
Institut de Ciència de Materials de Barcelona
ICMAB-CSIC, Campus UAB
Bellaterra E-08193, Spain

I. Zardo
Swiss Nanoscience Institute
University of Basel
Klingelbergstrasse 82, Basel CH-4056, Switzerland

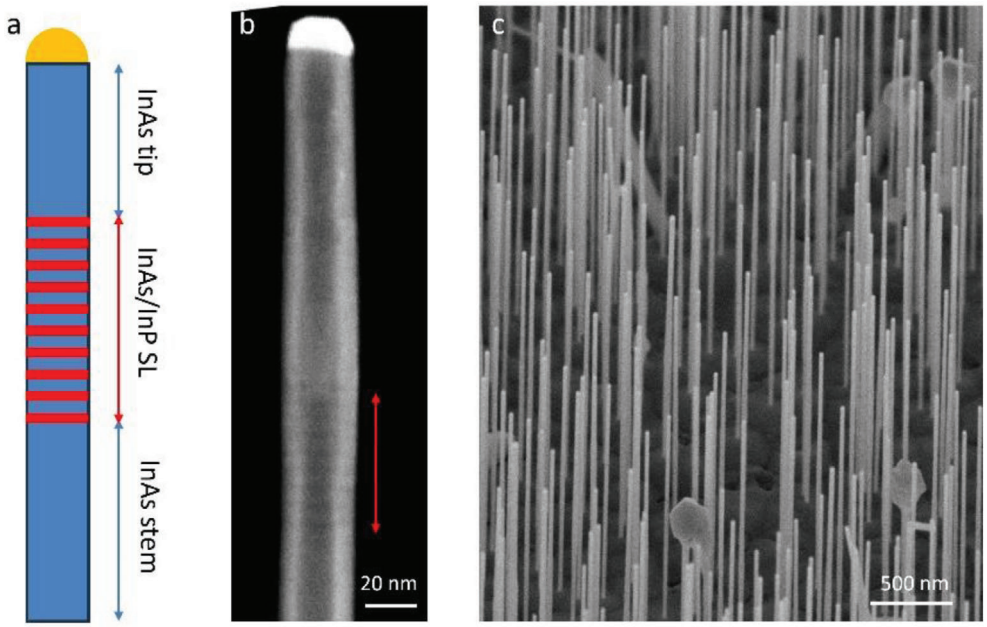

Figure 1. SL NW structure and morphology. a) Schematic representation of the SL NW structure composed of the InAs stem, the InAs/InP SL, and the InAs tip. Blue color represents InAs, while red color represents InP. b) SEM image of an individual NW of the calibration samples, transferred on a Si wafer. Red arrow indicates the SL portion, where the InP segments appear with darker contrast. c) 45°-tilted SEM image of the as-grown sample of NWs with SL made of 100 repetitions and periodicity of 4.8 nm.

The growth of dislocation-free heterostructures in NWs has been demonstrated also for highly lattice-mismatched materials,[16,17] representing an important degree of freedom in designing materials with tunable properties. Moreover, heterostructures with group V interchange having sharp interfaces can be obtained in NWs by means of the Au-assisted vapor-liquid-solid (VLS) growth,[18] thanks to the low solubility of group V elements into Au. Indeed, InAs/InP QD NWs with sharp interfaces between the two materials with outstanding optical[19] and electrical[20,21] properties have been achieved. Therefore, InAs/InP SL NWs of high crystal quality and variable periodicity represent a new class of materials for optoelectronic and thermoelectric applications. Remarkably, the high aspect ratio of NWs leads to an increase of phonon scattering at the lateral boundaries, strongly reducing the effective phonon mean free path with respect to the intrinsic value of the bulk material,[22] yielding an effective reduction of the thermal conductivity.[22–24] Moreover, the introduction of interfaces perpendicular to the growth axis should enhance the phonon scattering, while keeping unchanged the electron transport mechanisms, globally increasing the thermoelectric Figure of merit ZT.[23,25–27] To further investigate the impact of interface and surface scattering on the thermal properties of NWs, thermal conductivity measurements on SL NWs can be performed by the thermal bridge method[28,29] or the 3-ω method.[30,31] Also, the thermoelectric Figure of merit ZT of a NW can be quantified by combined micro-Raman (μ-Raman) and electric transport analysis.[32]

Here we report on the growth of Au-assisted InAs/InP SL NWs with well-defined segment thicknesses and periodicity, and we demonstrate the tunability of their phononic properties by inelastic light scattering experiments corroborated by ab initio calculations. We observe clear modifications in the dispersion relation, and we find that by controlling the superlattice periodicity we can achieve tunability of the phonon frequencies.

2. Results

It is known that both InAs/InP and InP/InAs interfaces in Au-assisted NWs suffer from growth delays and advances, due to the catalyst nanoparticle reconfiguration when switching from one material to the other one.[33] Therefore, initially, we grew several calibration samples with only 10 repetitions of the InAs/InP alternating segments, for different times, and we measured the segment thicknesses by scanning electron microscopy (SEM) imaging, to have an estimate of the actual growth rate of the two materials in thin alternating segments. Once calibrated the deposition times for both materials in the SL segment, we grew the final samples having 100 repetitions of the InAs/InP alternating segments in the SL. **Figure 1a** shows a schematic of the general NW structure. Figure 1b is a magnified image of a single NW of a calibration sample, transferred onto a Si substrate for performing high-resolution SEM imaging and thickness measurement. Figure 1c is instead a 45°-tilted SEM image of an as-grown final sample with the NWs having 100 InAs/InP repetitions in the SL segment. Depending on the SL periodicity, the average length of the NWs of the final samples varies between 1.9 and 2.5 μm, while the tip diameter of all of them is 30 ± 5 nm. Instead, the base diameter can be significantly different from sample to sample, because of the parasitic radial growth that occurs during the SL segment growth, resulting in NW tapering that is more pronounced as the InP segment thickness increases, as it will be explained later.

© 2024 The Authors. Advanced Physics Research published by Wiley-VCH GmbH

27511200, 0, Downloaded from https://onlinelibrary.wiley.com/doi/10.1002/apxr.202300157 by Scuola Normale Superiore Di Pisa, Wiley Online Library on [03/04/2024]. See the Terms and Conditions (https://onlinelibrary.wiley.com/terms-and-conditions) on Wiley Online Library for rules of use; OA articles are governed by the applicable Creative Commons License

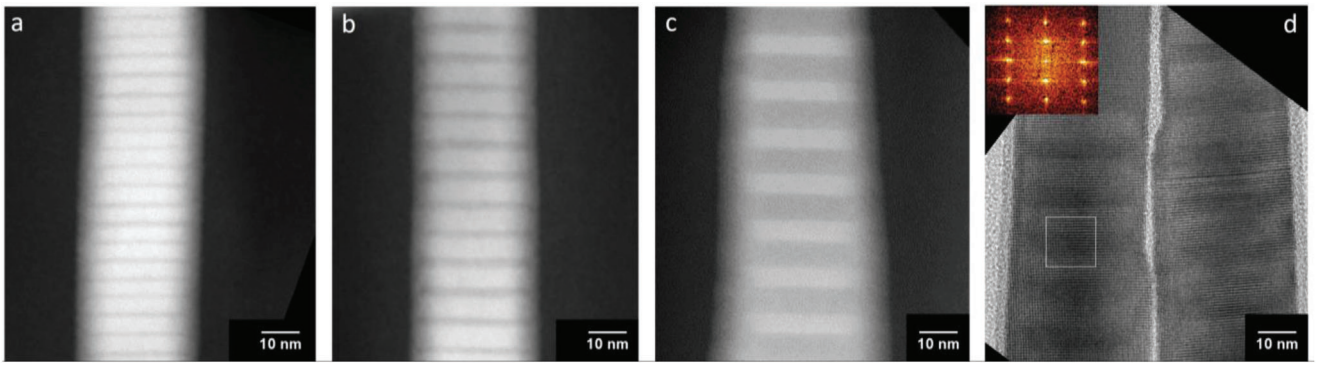

Figure 2. TEM analysis of the SL NWs. STEM images (a–c) of the upper portion of the SL segment of SL NWs with L = 4.8 nm a), L = 7.1 nm b), and L = 11.5 nm c). InP appears darker than InAs. d) Representative HRTEM image of SL NWs with L = 11.5 nm. The inset is the FFT of the white square frame that includes both InAs and InP segments and shows the WZ crystal structure in <2-1-10> zone axis.

Figure 2 summarizes the Transmission Electron Microscopy (TEM) analysis of three samples with different SL periodicity (L): L = 4.8 nm (1.5 nm InP and 3.3 nm InAs) in panel (a), L = 7.1 nm (2.3 nm InP and 4.8 nm InAs) in panel (b), L = 11.5 nm (6.5 nm InP and 5.0 nm InAs) in panels (c and d). From scanning-TEM (STEM) images like those shown in panels (a–c), we found that the InAs and InP segments are well-defined with sharp interfaces, with thicknesses that are quite homogeneous from the beginning to the end of the whole SL segment length, i.e., for all 100 repetitions, in all the samples. This means that in these growth conditions and for such NW length range, the axial growth rate is constant. On the other hand, we found that there is also a radial growth in the bottom part of the SL NWs, resulting in NW tapering, contrary to the pure InAs NWs of the same length. This tapering is more pronounced as the InP segment thickness, i.e., the InP deposition time, is increased (see Section S1, Supporting Information). This is probably because during the SL growth, the residual pressure in the growth chamber is higher, due to the use of both group-V precursors (tert-butyl arsine and tert-butyl phosphine) with high line pressures. Higher group-V fluxes are known to decrease the diffusion length of the In adatoms, resulting in a higher probability for them to nucleate on the NW sidewalls than reaching the catalyst nanoparticle on top.[34,35] This results indeed in NW tapering.

Panel (d) of Figure 2 shows a high-resolution TEM (HRTEM) image of the same sample depicted in (c): SL with L = 11.5 nm. Fast Fourier Transforms (FFT) of the images were taken from both the InAs segments and the InP segments of the SL (see inset), showing that both materials have a wurtzite (WZ) crystal structure. Moreover, all the SL NWs analyzed were almost free from stacking faults and twin planes, which are defects commonly observed in NWs grown along the <111> direction,[36] confirming their high crystal quality. In section S2 (Supporting Information), we also show an HRTEM image of the InAs/InP interface, together with its chemical analysis, confirming the interface abruptness and the chemical purity of the two materials.

We performed μ-Raman measurements on individual NWs of the three final samples depicted in Figure 2, transferred onto a gold-patterned silicon substrate. To form a comprehensive understanding of the modifications to the phonon spectrum in the SL NWs, we first compare the Raman spectrum of the 4.8 nm period SL NW with the spectra of pure WZ InAs and pure WZ InP reference NWs, as shown in **Figure 3a–c**. Here, the deconvolution of the experimental spectra with Lorentzian fitting is shown as solid lines along with the experimental data (open symbols).

Figure 3a shows the measured Raman spectrum of an InAs reference NW. The Raman peaks between 215 and 232 cm^{-1} are the transversal optical (TO) mode at ≈226 cm^{-1}, the longitudinal optical (LO) mode at ≈232 cm^{-1} and the E_2^H mode of WZ InAs at ≈215 cm^{-1}.[37,38] The InAs reference NW spectrum also shows three peaks below 140 cm^{-1} which can be attributed to the second-order acoustic modes. Moreover, we also observe a peak at ≈272 cm^{-1}, which is due to the mixture of transversal optical and transversal acoustic (TO+TA) modes.[39] In Figure 3b, the measured Raman spectrum of an InP reference NW is shown. There, three peaks can be seen: the TO mode of InP at ≈301 cm^{-1}, the $E_2{}^H$ mode of WZ InP at ≈303 cm^{-1} and the LO mode of InP at ≈343 cm^{-1}.[40] Figure 3c shows the measured Raman spectrum of a 4.8 nm period InAs-InP SL NW. Here we observe signals in the frequency range of both InAs and InP modes. For simplicity, from now on, the modes in the frequency range of InAs and InP will be called InAs-like and InP-like, respectively. The spectrum of the 4.8 nm period InAs-InP SL NW shows four phonon modes in the range from ≈94 to ≈140 cm^{-1}. We also observe a phonon mode at ≈272 cm^{-1} in the spectrum of the SL NW. The InAs-like modes are at ≈216, ≈226, and ≈232 cm^{-1}, while the InP-like modes are at ≈308 and ≈322 cm^{-1}. The InP-like SL modes are less intense compared to the InAs-like SL phonon modes. This difference in intensities is likely due to the fact that the 4.8 nm long SL period is composed of a longer InAs segment (3.3 nm) and a shorter InP segment (1.5 nm).

To better appreciate the presence of the InP-like SL modes, we plotted the spectra of the InAs and InP reference NWs and the SL NW in the frequency range from 250 to 330 cm^{-1} in Figure 3d, where one can clearly observe the InP-like SL phonon modes. In Figure 3e we present the calculated amplitude, A, of the atomic displacements for each Raman active mode as a function of the atomic index, n, for the 4.8 nm period InAs-InP SL NW obtained by density functional perturbation theory (DFPT) calculations.[41,42] The frequencies of the Raman active modes are reported in green on the right side. The InAs-like modes from 220.28 to 233.93 cm^{-1} involve only In and As atoms, while the InP-like modes from 313.6 to 323.24 cm^{-1} involve only In and P atoms. Comparing Figure 3c with the calculated Raman active

© 2024 The Authors. Advanced Physics Research published by Wiley-VCH GmbH

27511200, 0, Downloaded from https://onlinelibrary.wiley.com/doi/10.1002/apxr.202300157 by Scuola Normale Superiore Di Pisa, Wiley Online Library on [03/04/2024]. See the Terms and Conditions (https://onlinelibrary.wiley.com/terms-and-conditions) on Wiley Online Library for rules of use; OA articles are governed by the applicable Creative Commons License

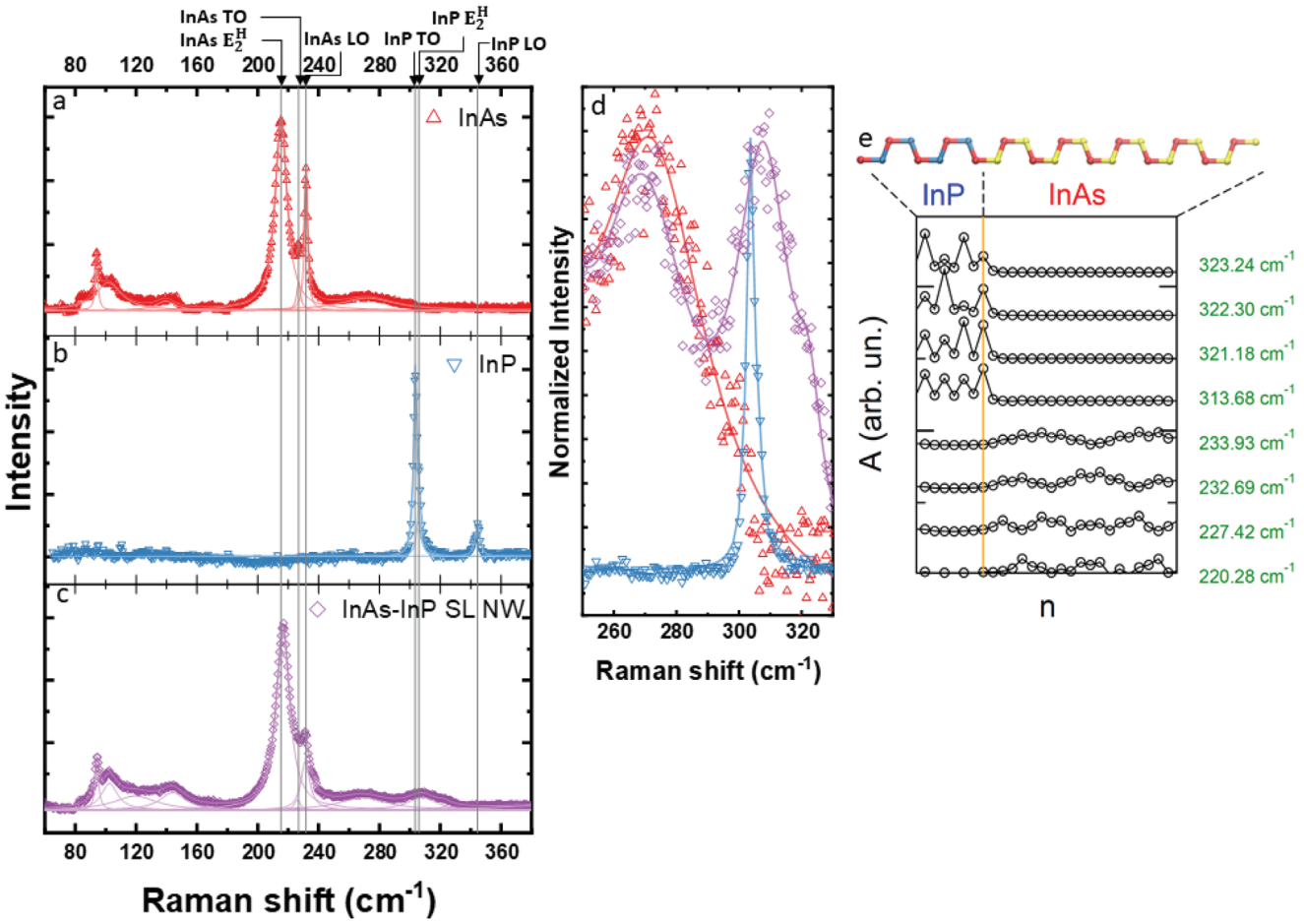

Figure 3. Measured Raman spectra of a) an InAs reference NW, b) an InP reference NW; c) a 4.8 nm period InAs–InP SL NW; each Raman spectrum was measured on a gold patterned substrate, and the background was subtracted. d) Detail of spectra of the InAs and InP reference NWs and of the 4.8 nm period SL NW in the frequency range from 250 to 330 cm^{-1}. e) Calculated amplitude, A, of the atomic displacements for each Raman active mode in the parallel polarization scattering geometry as a function of the atomic index, n (atoms 1 to 8 belong to InP, atoms 9 to 28 belong to InAs; the orange vertical line marks the position of the InP/InAs interface). The atomic structure of the unit cell is sketched in the upper panel (In, P, and As atoms are represented with red, blue, and yellow spheres, respectively). The frequencies of the modes are indicated on the right-hand side.

frequencies from Figure 3e, it can be seen that the experimentally measured modes agree well with the calculated modes. The InAs-like modes at 216, 226, and 232 cm^{-1} approximately coincide with the calculated Raman active modes at 220.28, 227.42, and 232.69 cm^{-1} and the InP-like modes at 308 and 322 cm^{-1} approximately coincide with the calculated Raman active modes at 313.68 and 322.30 cm^{-1}.

To investigate the tunability of the SL phonon modes, we performed μ-Raman measurements on the SL NWs with three different periodicities. **Figure 4** presents the overview of the results on the tunability of the phonon modes of the InAs–InP SL NWs. In Figure 4a–c, we show the Raman spectra from SL NW of periodicities (a) 4.8 nm, (b) 7.1 nm, and (c) 11.5 nm. Clearly, the InP-like modes are more prominent for the SL NW with a period of 11.5 nm, as compared to the SL NW with a period 4.8 and 7.1 nm. This can be explained as due to the differences in the SL composition, i.e., the SL NW with a period of 11.5 nm contains a longer InP segment than InAs segment compared to the other two periodicities. Consequently, the SL NWs with longer InP segments give a stronger signal from the InP-like modes, while the SL NWs with longer InAs layers give a stronger signal from the InAs-like modes. In Figure 4d, we plot the Raman spectra for the three SL NWs in the frequency range from 250 to 350 cm^{-1} to show the InP-like SL modes more clearly. In Figure 4e, we plot the phonon modes as a function of the SL periodicity. We see that as the SL periodicity increases, the number of phonon modes also increases. This can be explained by the increased number of atoms in the unit cell due to the increased SL period and by the reduction of the first Brillouin zone due to the longer lattice parameter with the resulting folding of the phonon bands.[43] Hence, more Raman modes appear for higher period thickness SLs.

3. Conclusion

In conclusion, we have grown WZ InAs NWs containing InAs/InP SLs of various periodicity with homogeneous segment thicknesses and sharp interfaces by means of Au-assisted Chemical Beam Epitaxy, and we have performed single-nanowire μ-Raman spectroscopy measurements, together with ab-initio DFT calculations. The experimentally measured Raman modes of the

© 2024 The Authors. Advanced Physics Research published by Wiley-VCH GmbH

27511200, 0, Downloaded from https://onlinelibrary.wiley.com/doi/10.1002/apxr.202300157 by Scuola Normale Superiore Di Pisa, Wiley Online Library on [03/04/2024]. See the Terms and Conditions (https://onlinelibrary.wiley.com/terms-and-conditions) on Wiley Online Library for rules of use; OA articles are governed by the applicable Creative Commons License

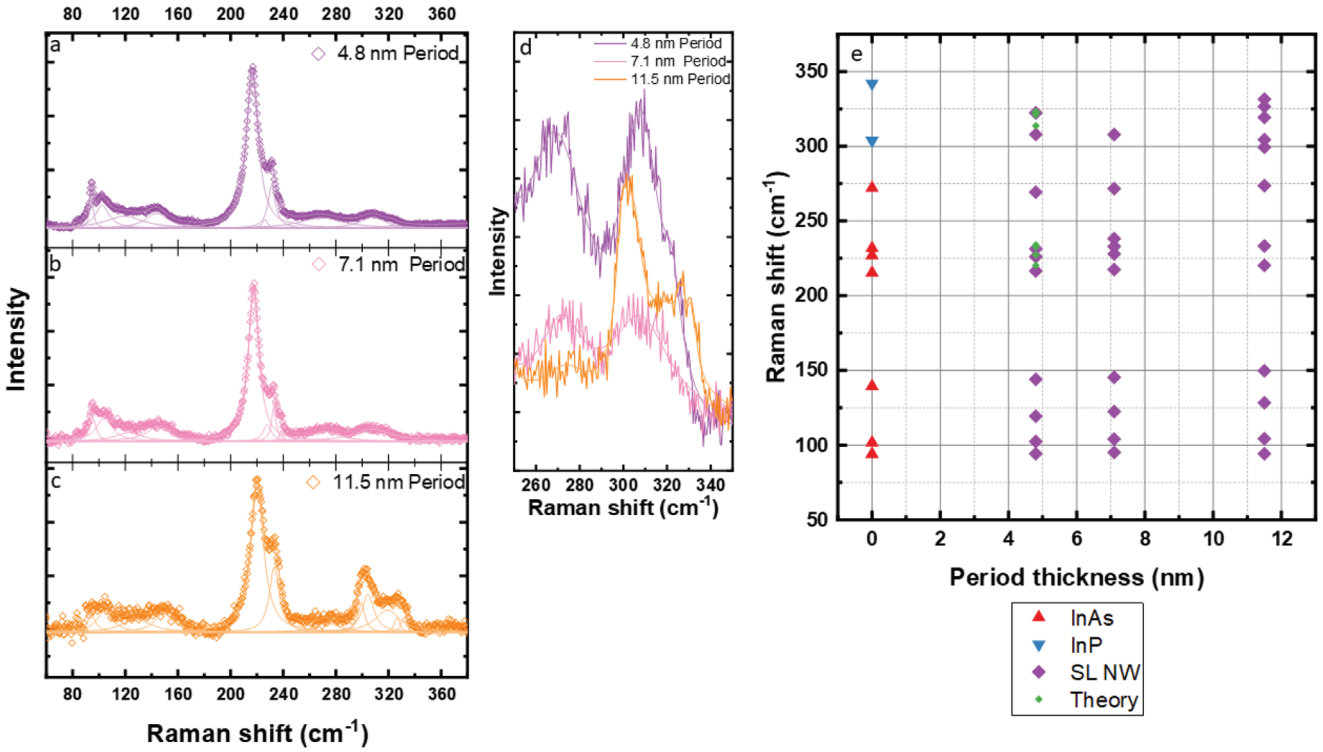

Figure 4. Raman spectra of SL NWs with a periodicity of a) 4.8 nm, b) 7.1 nm, and c) 11.5 nm, along with the deconvoluted Lorentz fitting. d) Spectra of the SL NWs in the frequency range from 250 to 350 cm^{-1}. e) Raman peak positions extracted from the experimental Raman spectra and theoretical calculations as a function of period thickness.

SL NWs agree well with the calculated modes. Most importantly, we have shown that the phonon frequencies and the number of phonons modes in the SL NWs can be tuned by varying the SL periodicity. This work demonstrates how material engineering at the nanoscale can tailor the phonon dispersion, opening exciting pathways for thermal management in semiconductor nanomaterials.

4. Experimental Section

The NWs were grown by means of Au-assisted VLS growth in a Riber C-21 chemical beam epitaxy (CBE) chamber on InAs(111)B substrates. The temperature was measured with an optical pyrometer, providing an overall accuracy of ±10 °C. Trimethylindium (TMIn), tert-butyl arsine (TBAs), and tert-butyl phosphine (TBP) were used as metalorganic precursors, with line pressures of 0.6, 1.5, and 1.5 Torr, respectively. The fluxes inside the chamber were triggered/stopped by opening/closing pneumatic valves located at the injectors, with an operation time scale of a few milliseconds, ensuring the absence of transient effects. Before mounting the substrate inside the CBE chamber, gold catalyst nanoparticles were deposited by colloid dispersion. Commercial water solutions of Au colloids with a nominal diameter of 20 nm (BBI Solutions) were drop-casted on the substrates, previously passivated with a poly-L-lysine 0.1% solution. The small nanoparticles,[44] together with the growth conditions used, ensure the growth of straight and pure WZ InAs/InP heterostructure NWs with sharp interfaces.[45] After degassing at 300 °C, the samples were transferred in the CBE chamber and the growth was started at 420 °C. InAs NW stems were first grown for 30 min. Subsequently, the InP/InAs alternating segments forming the SL were grown directly switching the As and P fluxes while keeping constant the In flux. Finally, an InAs tip was grown for 20 min. All the growth steps were performed at the same temperature, resulting in growth rates of 0.5 and 0.3 nm s^{-1} for InAs and InP NWs, respectively. At the end of the growth, the samples were cooled down at room temperature under As flux.

The samples were imaged with a SEM (Zeiss Merlin SEM) operating at 5 kV. TEM analysis was carried out using a JEOL JEM-2200FS, equipped with an in-column Ω filter, operated at 200 kV.

μ-Raman spectroscopy was performed on individual NWs transferred from the as-grown samples onto a gold-patterned silicon substrate. The Si substrate was coated with 525 nm of SiN_x followed by 3 nm of Ti and 27 nm of Au on the patterned regions. The Au substrate was used to enhance the Raman signal, similarly as in surface-enhanced Raman spectroscopy,[46,47] as well as to quench the Si background signal arising from the second order acoustic phonon modes in Si.[48] The μ-Raman measurements were performed in backscattering geometry using a Horiba T64000 triple spectrometer in subtractive mode with an 1800 g mm^{-1} grating and a liquid-nitrogen-cooled CCD detector. For the measurements, an excitation wavelength of 561 nm with a power on the sample of 100 μW was used. The incident light was polarized along the NW growth axis, which was considered the z-axis, and the incident and scattered photon wave vectors were anti-parallel to each other and directed along the x-axis, i.e., perpendicular to the plane onto which the NW was lying. Therefore, the scattering geometry used in this work can be written in conventional Porto notation as $\bar{x}(z, z)x$. The measurements were performed at room temperature using a 100× objective with a high numerical aperture of 0.95. The Γ-point frequencies and eigen displacements for the InAs/InP SL unit cell were computed by DFPT, within the local density approximation (LDA), with an energy cutoff of 40 Ha and a 16 × 16 × 2 k-point grid.

Supporting Information

Supporting Information is available from the Wiley Online Library or from the author.

© 2024 The Authors. Advanced Physics Research published by Wiley-VCH GmbH

27511200, 0, Downloaded from https://onlinelibrary.wiley.com/doi/10.1002/apxr.202300157 by Scuola Normale Superiore Di Pisa, Wiley Online Library on [03/04/2024]. See the Terms and Conditions (https://onlinelibrary.wiley.com/terms-and-conditions) on Wiley Online Library for rules of use; OA articles are governed by the applicable Creative Commons License

Acknowledgements

This project had received funding from the European Research Council (ERC) under the European Union's Horizon 2020 research and innovation program (grant agreement No 756365) and from the Swiss National Science Foundation grant (Grant No. 184942). V.Z. acknowledges financial support from the Italian Ministry of University and Research (MUR), PRIN project (grant No. 20223WZ245). R.R. acknowledges financial support by MCIN/AEI/10.13039/501100011033 under grant PID2020-119777GB-I00, and the Severo Ochoa Centres of Excellence Program under grant CEX2019-000917-S, and by the Generalitat de Catalunya under grant 2021 SGR 01519. The authors thank the Centro de Supercomputación de Galicia (CESGA) for the use of their computational resources. A.K.S. acknowledges financial support from the Georg H. Endress foundation. B.A. acknowledges support from the European Union's Horizon 2020 research and innovation programme under the Marie Skłodowska-Curie Grant Agreement No. 891443.

Conflict of Interest

The authors declare no conflict of interest.

Data Availability Statement

The data that support the findings of this study are openly available in ZENODO at https://doi.org/10.5281/zenodo.10666956, reference number 10666956.

Keywords

InAs–InP, phononic properties, phonons, Raman spectroscopy, superlattice nanowires

Received: December 22, 2023
Revised: February 19, 2024
Published online:

[1] H. J. Joyce, Q. Gao, H. Hoe Tan, C. Jagadish, Y. Kim, J. Zou, L. M. Smith, H. E. Jackson, J. M. Yarrison-Rice, P. Parkinson, M. B. Johnston, *Prog. Quantum Electron.* **2011**, *35*, 23.
[2] J. Wong-Leung, I. Yang, Z. Li, S. K. Karuturi, L. Fu, H. H. Tan, C. Jagadish, *Adv. Mater.* **2020**, *32*, 1904359.
[3] F. Glas, *Phys. Rev. B* **2006**, *74*, 2.
[4] M. N. Luckyanova, J. Garg, K. Esfarjani, A. Jandl, M. T. Bulsara, A. J. Schmidt, A. J. Minnich, S. Chen, M. S. Dresselhaus, Z. Ren, E. a Fitzgerald, G. Chen, *Science* **2012**, *338*, 936.
[5] J. Ravichandran, A. K. Yadav, R. Cheaito, P. B. Rossen, A. Soukiassian, S. J. Suresha, J. C. Duda, B. M. Foley, C. H. Lee, Y. Zhu, A. W. Lichtenberger, J. E. Moore, D. A. Muller, D. G. Schlom, P. E. Hopkins, A. Majumdar, R. Ramesh, M. A. Zurbuchen, *Nat. Mater.* **2014**, *13*, 168.
[6] M. Maldovan, *Nat. Mater.* **2015**, *14*, 667.
[7] T. Borca-Tasciuc, W. Liu, J. Liu, T. Zeng, D. W. Song, C. D. Moore, G. Chen, K. L. Wang, M. S. Goorsky, T. Radetic, R. Gronsky, T. Koga, M. S. Dresselhaus, *Superlattices Microstruct.* **2000**, *28*, 199.
[8] J. F. Klem, S. R. Kurtz, A. Datye, *J. Cryst. Growth* **1991**, *111*, 628.
[9] H. K. Shin, D. J. Lockwood, P. J. Poole, *Appl. Phys. Lett.* **2000**, *77*, 229.
[10] A. Rogalski, P. Martyniuk, M. Kopytko, *Appl. Phys. Rev.* **2017**, *4*, 031304.
[11] B.-W. Zhang, D. Fang, X. Fang, H.-B. Zhao, D.-K. Wang, J.-H. Li, X.-H. Wang, D.-B. Wang, *Rare Met.* **2022**, *41*, 982.
[12] C. A. Tran, M. Jouanne, J. L. Brebner, R. A. Masut, *J. Appl. Phys.* **1993**, *74*, 4983.
[13] A. Continenza, S. Massidda, A. J. Freeman, *Phys. Rev. B* **1990**, *41*, 12013.
[14] T. K. Woodward, T. Sizer, T. H. Chiu, *Appl. Phys. Lett.* **1991**, *58*, 1366.
[15] S. Mokkapati, C. Jagadish, *Mater. Today* **2009**, *12*, 22.
[16] P. Caroff, M. E. Messing, B. M. Borg, K. A. Dick, K. Deppert, L. E. Wernersson, *Nanotechnology* **2009**, *20*, 495606.
[17] D. V. Beznasyuk, E. Robin, M. Den Hertog, J. Claudon, M. Hocevar, *Nanotechnology* **2017**, *28*, 365602.
[18] K. A. Dick, *Prog. Cryst. Growth Charact. Mater.* **2008**, *54*, 138.
[19] S. Haffouz, K. D. Zeuner, D. Dalacu, P. J. Poole, J. Lapointe, D. Poitras, K. Mnaymneh, X. Wu, M. Couillard, M. Korkusinski, E. Schöll, K. D. Jöns, V. Zwiller, R. L. Williams, *Nano Lett.* **2018**, *18*, 3047.
[20] F. S. Thomas, A. Baumgartner, L. Gubser, C. Jünger, G. Fülöp, M. Nilsson, F. Rossi, V. Zannier, L. Sorba, C. Schönenberger, *Nanotechnology* **2020**, *31*, 135003.
[21] T. Elalaily, O. Kürtössy, V. Zannier, Z. Scherübl, I. E. Lukács, P. Srivastava, F. Rossi, L. Sorba, S. Csonka, P. Makk, *Phys. Rev. Appl.* **2020**, *14*, 044002.
[22] L. Hicks, M. S. Dresselhaus, *Phys. Rev. B* **1993**, *47*, 8.
[23] Y. M. Lin, S. Dresselhaus, *Phys. Rev. B* **2003**, *68*, 075304.
[24] R. Chen, J. Lee, W. Lee, D. Li, *Chem. Rev.* **2019**, *119*, 9260.
[25] D. Li, Y. Wu, R. Fan, P. Yang, A. Majumdar, *Appl. Phys. Lett.* **2003**, *83*, 3186.
[26] L. Peri, D. Prete, V. Demontis, V. Zannier, F. Rossi, L. Sorba, F. Beltram, F. Rossella, *Nano Energy* **2022**, *103*, 107700.
[27] A. K. Sivan, B. Abad, T. Albrigi, O. Arif, J. Trautvetter, A. Ruiz Caridad, C. Arya, V. Zannier, L. Sorba, R. Rurali, I. Zardo, *ACS Appl. Nano Mater.* **2023**, *6*, 18602.
[28] L. Shi, D. Li, C. Yu, W. Jang, D. Kim, Z. Yao, P. Kim, A. Majumdar, *J. Heat Transfer* **2003**, *125*, 881.
[29] D. Vakulov, S. Gireesan, M. Y. Swinkels, R. Chavez, T. Vogelaar, P. Torres, A. Campo, M. De Luca, M. A. Verheijen, S. Koelling, L. Gagliano, J. E. M. Haverkort, F. X. Alvarez, P. A. Bobbert, I. Zardo, E. P. A. M. Bakkers, *Nano Lett.* **2020**, *20*, 2703.
[30] J. Kimling, S. Martens, K. Nielsch, *Rev. Sci. Instrum.* **2011**, *82*, 074903.
[31] M. Rocci, V. Demontis, D. Prete, D. Ercolani, L. Sorba, F. Beltram, G. Pennelli, S. Roddaro, F. Rossella, *J. Mater. Eng. Perform.* **2018**, *27*, 6299.
[32] S. Yazji, E. A. Hoffman, D. Ercolani, F. Rossella, A. Pitanti, A. Cavalli, S. Roddaro, G. Abstreiter, L. Sorba, I. Zardo, *Nano Res.* **2015**, *8*, 4048.
[33] V. Zannier, F. Rossi, D. Ercolani, L. Sorba, *Nanotechnology* **2019**, *30*, 094003.
[34] M. C. Plante, R. R. LaPierre, *J. Cryst. Growth* **2008**, *310*, 356.
[35] S. Paiman, Q. Gao, H. J. Joyce, Y. Kim, H. H. Tan, C. Jagadish, X. Zhang, Y. Guo, J. Zou, *J. Phys. D. Appl. Phys.* **2010**, *43*, 445402.
[36] J. Johansson, L. S. Karlsson, C. P. T. Svensson, T. Mårtensson, B. A. Wacaser, K. Deppert, L. Samuelson, W. Seifert, *Nat. Mater.* **2006**, *5*, 574.
[37] M. Möller, M. M. De Lima, A. Cantarero, L. C. O. Dacal, J. R. Madureira, F. Iikawa, T. Chiaramonte, M. A. Cotta, *Phys. Rev. B* **2011**, *84*, 085318.
[38] S. D. Dabhi, P. K. Jha, *J. Phys. Chem. Solids* **2015**, *83*, 70.
[39] R. Carles, N. Saint-Cricq, J. B. Renucci, M. A. Renucci, A. Zwick, *Phys. Rev. B* **1980**, *22*, 4804.
[40] E. Bedel1, G. Landa1, R. Carles1, J. P. Redoulès, J. B. Renucci, *J. Phys. C Solid State Phys.* **1986**, *19*, 1471.
[41] S. Baroni, S. De Gironcoli, A. Dal Corso, P. Giannozzi, *Rev. Mod. Phys.* **2001**, *73*, 515.
[42] X. Gonze, B. Amadon, P. M. Anglade, J. M. Beuken, F. Bottin, P. Boulanger, F. Bruneval, D. Caliste, R. Caracas, M. Côté, T. Deutsch, L. Genovese, P. Ghosez, M. Giantomassi, S. Goedecker, D. R. Hamann,

© 2024 The Authors. Advanced Physics Research published by Wiley-VCH GmbH

27511200, 0, Downloaded from https://onlinelibrary.wiley.com/doi/10.1002/apxr.202300157 by Scuola Normale Superiore Di Pisa, Wiley Online Library on [03/04/2024]. See the Terms and Conditions (https://onlinelibrary.wiley.com/terms-and-conditions) on Wiley Online Library for rules of use; OA articles are governed by the applicable Creative Commons License

P. Hermet, F. Jollet, G. Jomard, S. Leroux, M. Mancini, S. Mazevet, M. J. T. Oliveira, G. Onida, Y. Pouillon, T. Rangel, G. M. Rignanese, D. Sangalli, R. Shaltaf, M. Torrent, *Comput. Phys. Commun.* **2009**, *180*, 2582.

[43] B. Jusserand, M. Cardona, in *Light Scattering in Solids V: Superlattices and Other Microstructures* (Eds: M. Cardona, G. Güntherodt), Springer, Berlin **1989**.

[44] E. K. Mårtensson, S. Lehmann, K. A. Dick, J. Johansson, *Cryst. Growth Des.* **2020**, *20*, 5373.

[45] V. Zannier, F. Rossi, V. G. Dubrovskii, D. Ercolani, S. Battiato, L. Sorba, *Nano Lett.* **2018**, *18*, 167.

[46] N. Y. Kim, M. K. Oh, S. H. Park, S. K. Kim, B. H. Hong, *Bull. Korean Chem. Soc.* **2010**, *31*, 999.

[47] R. E. Littleford, D. Graham, W. E. Smith, I. Khan, *Surface-Enhanced Raman Scattering (SERS), Applications, in Encyclopedia of Spectroscopy and Spectrometry* (Eds: J. C. Lindon, G. E. Tranter, D. W. Koppenaal), Academic Press, Oxford **2017**, pp. 389-395.

[48] J. B. Renucci, R. N. Tyte, M. Cardona, *Phys. Rev. B* **1975**, *11*, 3885.

© 2024 The Authors. Advanced Physics Research published by Wiley-VCH GmbH

27511200, 0, Downloaded from https://onlinelibrary.wiley.com/doi/10.1002/apxr.202300157 by Scuola Normale Superiore Di Pisa, Wiley Online Library on [03/04/2024]. See the Terms and Conditions (https://onlinelibrary.wiley.com/terms-and-conditions) on Wiley Online Library for rules of use; OA articles are governed by the applicable Creative Commons License